Inorganic Chemistry
Article
pubs.acs.org/IC

Supramolecular Control over Molecular Magnetic Materials: γ-Cyclodextrin-Templated Grid of Cobalt(II) Single-Ion Magnets

Natalia Nedelko,[†,‡] Arkadiusz Kornowicz,[§,‡] Iwona Justyniak,[⊥] Pavlo Aleshkevych,[†] Daniel Prochowicz,[§] Piotr Krupiński,[⊥] Orest Dorosh,[∥] Anna Ślawska-Waniewska,[*,†] and Janusz Lewiński[*,§,⊥]

[†]Institute of Physics, Polish Academy of Sciences, al. Lotników 32/46, 02-668 Warsaw, Poland

[§]Department of Chemistry, Warsaw University of Technology, Noakowskiego 3, 00−664 Warsaw, Poland

[⊥]Institute of Physical Chemistry, Polish Academy of Sciences, Kasprzaka 44/52, 01-224 Warsaw, Poland

[∥]National Center for Nuclear Research, ul. Sołtana 7, 05-400 Otwock, Poland

Supporting Information

ABSTRACT: Single-ion magnets (SIMs) are potential building blocks of novel quantum computing devices. Unique magnetic properties of SIMs require effective separation of magnetic ions and can be tuned by even slight changes in their coordination sphere geometry. We show that an additional level of tailorability in the design of SIMs can be achieved by organizing magnetic ions into supramolecular architectures, resulting in gaining control over magnetic ion packing. Here, γ-cyclodextrin was used to template magnetic Co^{II} and nonmagnetic auxiliary Li^+ ions to form a heterometallic {Co, Li, Li}$_4$ ring. In the sandwich-type complex $[(\gamma\text{-CD})_2Co_4Li_8(H_2O)_{12}]$ spatially separated Co^{II} ions are prevented from superexchange magnetic coupling. Ac/dc magnetic and EPR studies demonstrated that individual Co^{II} ions with positive zero-field splitting exhibit field-induced slow magnetic relaxation consistent with the SIMs' behavior, which is exceptional in complexes with easy-plane magnetic anisotropy.

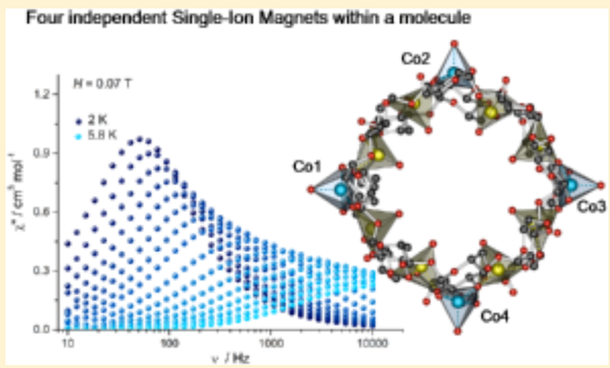

INTRODUCTION

During the last two decades we have been witnessing rapid development in the field of single-molecule magnets (SMMs).[1] SMMs demonstrate slow relaxation of magnetic moments after removing an external magnetic field as well as allow observations of quantum tunneling of magnetization (QTM) and quantum phase interference effects and as such have been suggested for applications in high-density information storage and quantum spintronics.[1] The early reported examples of SMMs were multinuclear aggregates of high-spin 3d metal ions, whereas later multidimensional networks of SMMs were also developed.[2] Recently, there is particular interest in molecular systems with only one spin carrier, large Ising-type magnetic anisotropy, and properties consistent with SMMs termed single-ion magnets (SIMs). Most of the reported SIMs contain late lanthanide ions ($4f^n$, $n > 7$),[3] and only a few examples of SIMs containing first-row transition metals are known, i.e., Co^{II} complexes with different geometries,[4] Mn^{III},[5] Ni^{I},[6] and Fe^{II}[7] and Fe^{III}[8] complexes. The design of SIMs creates new challenges, as magnetic ions, with suitable local magnetic anisotropy, need to be effectively separated from each other and even small changes in metal−ligand interactions can have a great impact on magnetic properties.[4a,d,e,7b,e] An additional level of tailorability in the design of SIMs can be achieved by organizing magnetic ions into supramolecular architectures, resulting in gaining control over magnetic ion packing along with elimination of magnetic interactions. Thus, we turned our attention to cyclodextrins (CDs) as site-directing ligands with the aim of designing a system in which magnetic metal ions will be densely packed but at the same time sufficiently spatially separated in order to prevent superexchange magnetic coupling. Although the chemistry of CD−metal complexes is relatively unexplored due to the difficulties with the isolation of well-defined systems, CDs have already served as templates for metal ions enabling the formation of supramolecular systems with a variety of intriguing properties.[9] Deprotonation of hydroxyl groups and coordination of metal ions to CDs has led to the fabrication of cylindrical, extended structures[9b,c] or sandwich-type complexes[9a,e,f,h] depending on the character of the metal ion. The very rare examples of heterometallic sandwich-type complexes of CDs indicate that utilizing Na^+ as auxiliary ions leads to the formation of a {M, Na}$_n$ metallamacrocycle with alternate metal centers.[9b,e] On the contrary, Li^+ as auxiliary ions is potentially able to promote the formation of {M, Li, Li}$_n$-type rings.[9a,c] Among these heterometallic sandwich-type complexes, there is only one CD metal complex with the reported magnetic properties, namely, $Na_7(V{=}O)_7Na_7(H_2O)_7(\beta\text{-CD})_2{\cdot}nH_2O$

Received: July 31, 2014
Published: November 19, 2014

dx.doi.org/10.1021/ic501870h | *Inorg. Chem.* 2014, 53, 12870−12876

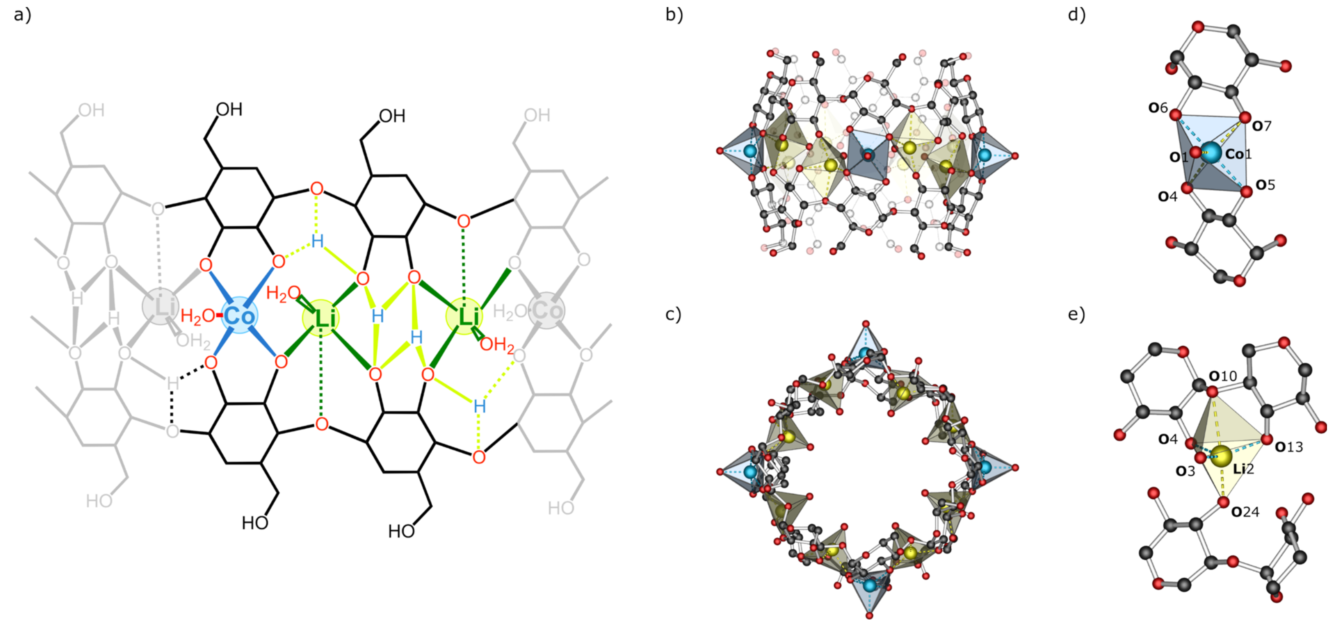

Figure 1. Molecular structure of **1**: (a) representation of H-bond system in the heterometallic ring {Co, Li, Li} unit in **1**. Side view (b) and top view (c). Coordination sphere of the Co^{2+} (d) and Li^{+} (e) ions.

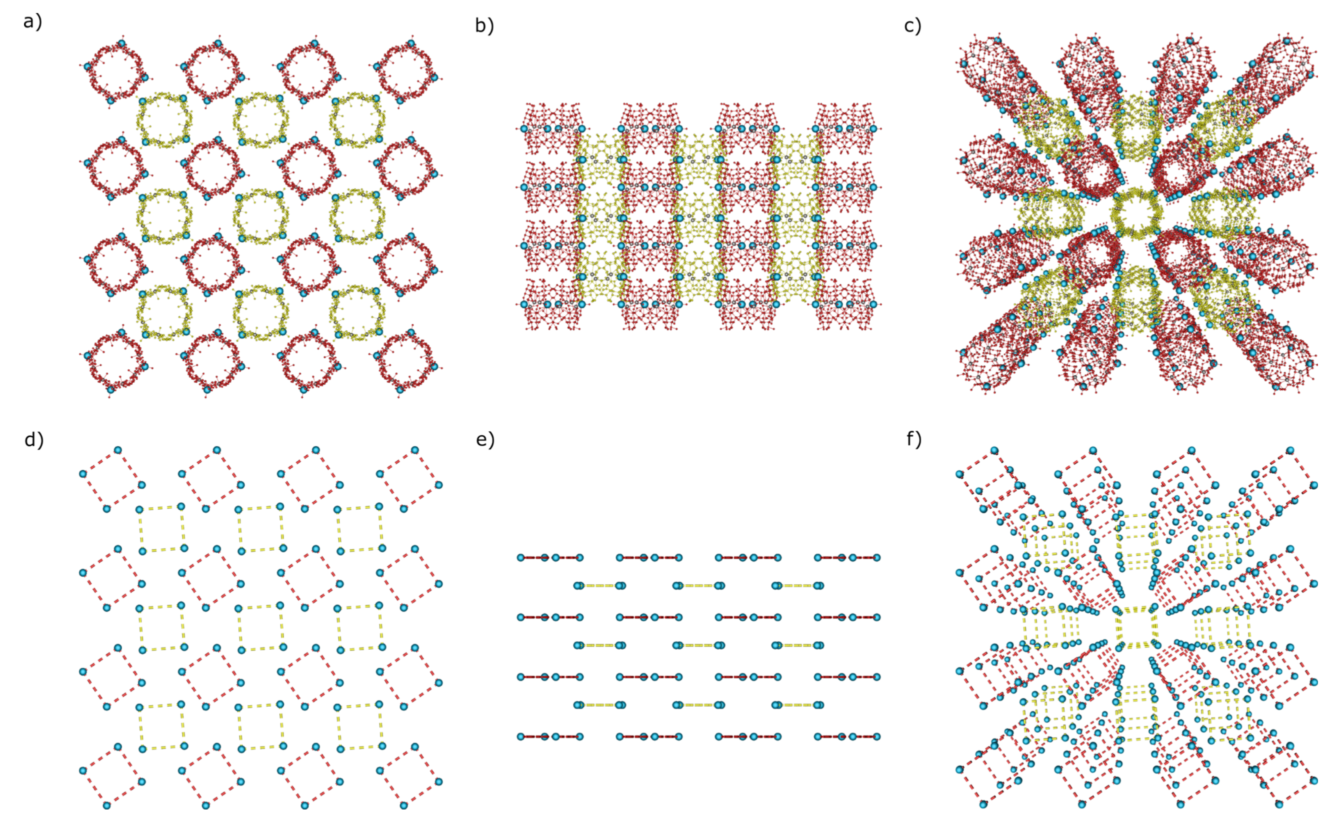

Figure 2. Supramolecular structure of **1**: view along the *c* axis (a) and *a* axis (b) and arrangement of Co^{2+} ions along the *c* axis (d) and *a* axis (e). (c) Stacked view along the *c* axis showing the formation of pillar-like structures. (f) Arrangement of Co^{2+} ions in the structure of **1**; Co^{2+} ions stacked along the *c* axis.

(where the oxo-vanadate ions are separated by a single Na^+ ion), in which relatively short V⋯V distances lead to an antiferromagnetic ordering within the heterometallic ring.[9e] With this in mind, we explored a reaction system involving γ-CD, $CoCl_2$, and LiOH that could lead to the formation of a $\{Co, Li, Li\}_n$-type ring with ultimately increased magnetic ion M⋯M separation. Herein, we report the synthesis, structure characterization, and magnetic behavior of a novel heterometallic dodecanuclear sandwich-type complex, $[(\gamma\text{-CD})_2Co_4Li_8(H_2O)_{12}]$ (**1**), containing a $\{Co, Li, Li\}_4$ ring. We demonstrate that (i) individual Co^{II} ions in **1** exhibit a field-induced slow magnetic relaxation consistent with the SIM behavior, and as such, the presented system is a unique example of a grid of four Co^{II}-based SIMs replicated in supramolecular architecture, and (ii) the magnetic Co^{II} ions are endowed with a positive value of zero-field splitting (ZFS) parameter D. While a few examples of Co^{II}-based SIMs with easy-plane anisotropy ($D > 0$) are known,[4c,g,h,j,k] the mechanisms responsible for such behavior still remain unclear,[4k] and we also address this issue in our investigations.

■ RESULTS AND DISCUSSION

Synthesis and Structure. The heterometallic cobalt−lithium−γ-CD complex was prepared by combining γ-CD with $CoCl_2$ and LiOH in aqueous solution at room temperature. From a deep blue solution well-formed pink needle-like crystals of $[(\gamma\text{-CD})_2Co_4Li_8(H_2O)_{12}]$ (**1**) were grown within 2 weeks by slow diffusion of acetone vapors. Single-crystal X-ray diffraction reveals that **1** crystallizes in the *P*4 space group, and its molecular structure is based on two eight times deprotonated γ-CD molecules connected through a dodeca-membered heterometallic ring forming a double-toroidal structure (Figure 1). The metallamacrocycle consists of four Co^{II} and eight Li^{I} ions grouped in four {Co, Li, Li} units. Each Co^{II} center adopts distorted trigonal bipyramidal geometry with the CoO_5 environment (Figure 1d); the tau parameter describing the distortion from ideal trigonal bipiramidal geometry was estimated as 0.69−0.72 for different Co^{II} centers. The equatorial plane is defined by two $O_{alkoxide}$ and one O_{water} atoms with O−Co−O angles ranging from 109.8(2)° to 133.7(2)°. The axial positions are occupied by two secondary hydroxyl groups with angles of 175.3(2)−173.5(2)°. The equatorial Co−O bond distances (1.996(5) to 2.045(5) Å) are slightly shorter than the axial Co−O bond distances (2.117(5) to 2.144(5) Å). Notably, Co^{II} centers are located in the plane resembling a square with intramolecular Co···Co distances of 10.7−10.9 Å. Every Li^{I} ion in **1** binds a water molecule directed toward the channel space (*vide infra*) and adopts distorted trigonal bipyramidal geometry with two $O_{alkoxide}$, one O_{ether}, one $O_{hydroxyl}$, and one O_{water} oxygen atom (Figure 1e). The oxygen atoms of eight water molecules bound to Li^{I} ions are the basis of a $(H_2O)_8$ truncated square. In the crystal structure molecules of **1** extend infinitely along the *c* axis, forming pillar-like structures stabilized by water-mediated H-bonds, which results in the formation of 1D open channels (Figure 2a and c) filled by water molecules. The Co^{II} ions in the heterometallic rings are arranged in straight lines parallel to the *c* axis with distances of 15.36 Å (Figure 2d and e). Hydrogen bond interactions also support molecular shape-driven assembly along the *a* and *b* axes into tight 2D layers (Figure 2a). The neighboring columns are translated along the *a* axis by 7.22 Å and twisted by an angle of 35°, which improves the intermolecular separation of Co^{II} ions with the shortest Co···Co distance of 9.63 Å.

Magnetic Behavior. The results of dc magnetic investigations for **1** are typical of paramagnets: (i) a Curie−Weiss law for magnetic susceptibility ($\chi = M/H$) is fulfilled in the temperature range 20−298 K; (ii) the thermal dependences of ZFC and FC magnetization, measured at $H = 0.1$ T applied magnetic field, superimpose in the whole measured temperature range; (iii) $M(H)$ curves, taken at 2, 3, 4, and 5 K in a ±9 T field, demonstrate zero coercivity. The dynamic ac susceptibility measurements at zero static magnetic field H confirm the paramagnetic behavior of the studied system: the thermal evolutions of the in-phase susceptibility component (χ') reveal no frequency dependence and a complete absence of the out-of-phase component (χ''). For further analysis, we chose $\chi'(T)$ dependence measured in an oscillating ($\nu = 5$ kHz) ac field of 5 Oe at $H = 0$; see Figure 3 for $\chi'T$ vs T plot. At

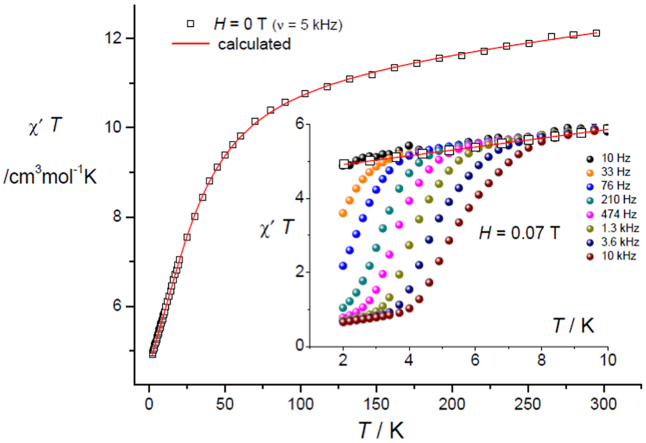

Figure 3. Temperature dependence of $\chi'T$ product in zero dc magnetic field: experimental results (symbols) and simulation using a spin-Hamiltonian for mononuclear model (solid line). Inset: Variable-frequency $\chi'T(T)$ curves obtained in 0.07 T dc field and at different ac field frequencies (for comparison, the frequency-independent $\chi'T(T)$ curve for $H = 0$ T is also included).

room temperature $\chi'T$ = 12.12 cm^3 mol^{-1} K, which is consistent with the presence of four magnetically isolated high-spin Co^{II} centers with significant spin−orbit contributions. The $\chi'T$ product decreases substantially below 70 K down to 4.92 cm^3 mol^{-1} K at 2 K. The near saturation magnetic moment measured at 2 K (in 9 T) is 1.7 μ_B per Co ion, which is within the range (1.5−2.5 μ_B) expected for randomly oriented highly anisotropic magnetically isolated Co^{II} complexes.[10] Therefore, the decreasing $\chi'T$ values upon cooling, lack of superposition of $M(H/T)$ curves, and unsaturation of $M(H)$ in 9 T at very low temperatures (Figure S1) can be related to significant single-ion magnetic anisotropy. The ground term of free d^7 ions is ^{4}F. In the D_{3h} symmetry this 7-fold degenerate term breaks up into $^4A'_2$, ($^4A''_1$+$^4A''_2$), $^4E''$, and $^4E'$ states (in the angular overlap model formalism), and the lowest is the $^4A'_2$ orbital singlet with 4-fold spin multiplicity. The combined effect of both the crystal field and spin−orbit coupling causes splitting of the $^4A'_2$ ground state into two Kramers doublets, which, for simplicity, can be loosely described through the spin quantum numbers m_S as ±1/2 and ±3/2. The observed magnetic properties of **1** are solely determined by these two doublets, as they are the only populated energy levels at $T <$ 300 K. The mononuclear spin quadruplet can be described by a phenomenological spin-Hamiltonian that includes the Zeeman and ZFS terms in the form [eq (a)] $\mathcal{H} = \mu_B H\cdot g\cdot\hat{S} + D[\hat{S}_z^2 - S(S+1)/3] + E[\hat{S}_x^2 - \hat{S}_y^2]$ (a), where D and E are the axial and rhombic ZFS parameters, respectively. The experimental temperature dependence of the magnetic susceptibility of **1** was analyzed within the above spin-Hamiltonian. The best fit was obtained for D = +27.9 cm^{-1}, E = −6.3 cm^{-1},[11] g_z = 2.7, g_x = 1.7, g_y = 2.8, and χ_{TIP} = +0.9 × 10^{-3}, with the agreement factor $R \approx 1 \times 10^{-7}$ (solid line in Figure 3; see Experimental Section for details). Accordingly, m_S = ±1/2 doublet is the ground state, and the separation between m_S = ±1/2 and m_S = ±3/2 doublets is $2(D^2 + 3E^2)^{1/2} \approx 60$ cm^{-1}. The best-fit values of ZFS parameters are consistent with the results of the EPR

dx.doi.org/10.1021/ic501870h | Inorg. Chem. 2014, 53, 12870−12876

experiment for a polycrystalline powdered sample at 3.7 K (Figure S2). Notably the estimated value and sign of D correlate well with those predicted by the theory and confirmed experimentally for cobalt complexes with similar geometry.[4e,12] The considerable rhombicity $|E/D|$ is usually attributed to the deviations of magnetic ion environments from ideal geometry. As in **1** the distortion factor seems to be not very significant, two additional effects can be responsible for the relatively large $|E/D| \approx 0.22$ value: (a) the nonequivalence of the ligands in equatorial positions and the special role of coordinated water molecules[13] or (b) the effect of the second coordination sphere, which was already evidenced for Co^{II}.[14]

In order to gain more in-depth insight into the intrinsic anisotropy of **1**, we performed the dynamic ac susceptibility measurements as a function of temperature and frequency in different external static fields H (in the range 0.01−0.7 T). The results demonstrate features typical of a phenomenon known as slow magnetic relaxation: the appearance of a nonzero out-of-phase χ'' component, the emergence of the frequency-dependent maximum on both $\chi'(T)$ and $\chi''(T)$ curves (Figure 3, inset, and Figure S3), and the maximum on $\chi''(\nu)$ dependences at very low temperatures (Figure S4 and Figure 4). For a given H and T = 2 K the Cole−Cole plots were

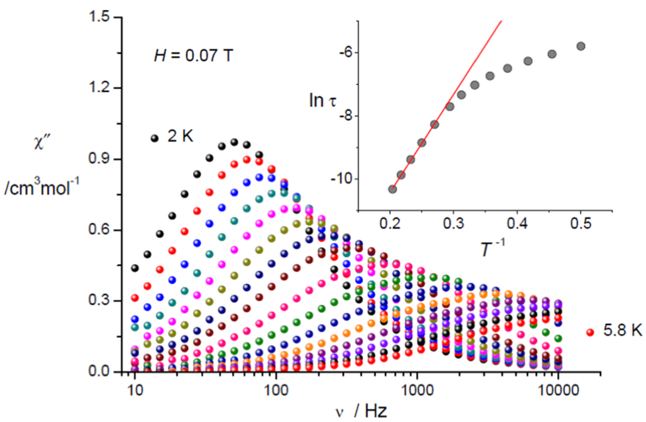

Figure 4. Frequency dependences of the out-of-phase ac susceptibility, χ'', obtained at temperatures between 2 and 5.8 K in a 0.07 T dc magnetic field. Inset: Arrhenius plot of the relaxation time and a linear fit.

constructed and fitted to a generalized Debye model with a single relaxation process.[15] For example, the semicircular Cole−Cole plot for H = 0.07 T is shown in Figure 5 (inset), the appropriate plots for other dc fields are presented in Figure S5, and the values of fitted parameters are given in Table S1. The estimated relaxation time at 2 K displays strong field dependence (Figure 5).

To explore thermal dependence of the relaxation time, isothermal ac frequency scans in 0.07 T were performed (Figure 4). H = 0.07 T was chosen, as it induces the largest amplitude of the out-of-phase component and the slowest relaxations at 2 K. The values of the magnetic relaxation times, extracted from appropriate Cole−Cole plots (Figure S6 and Table S2), are presented in the form of the Arrhenius plot in Figure 4 (inset). The linear behavior of ln τ vs $(1/T)$ for T > 3.5 K shows that with increasing temperature the system follows the Arrhenius law, $\tau = \tau_0 \exp(U_{eff}/k_BT)$. The appropriate fitting procedure (Figure 4, solid line in the inset) gives the average values of U_{eff} = 21.5 cm $^{-1}$ and τ_0 = 6.2 $\times 10^{-8}$ s for the spin-reversal barrier and attempt time, respectively. The value of the pre-exponential factor, τ_0, is within the range typical of SIMs (1×10^{-7} to 1×10^{-11} s) and 3 orders of magnitude smaller than observed for the phonon bottleneck Orbach relaxation processes.[16] Therefore, we suggest SIM behavior as the source of the observed field-induced slow relaxation in **1**. In addition, the obtained value of the energy barrier (21.5 cm $^{-1}$) is significantly smaller than the splitting energy of two lowest Kramers doublets (60 cm $^{-1}$) derived from the magnetic and EPR studies. This fact distinguishes the slow magnetic relaxation mechanism observed in **1** from that reported by Zadrozny et al. for a tetrahedral Co^{II} complex (in the latter system a phonon bottleneck effect led to Orbach relaxations over the energy barrier corresponding to ±1/2 and ±3/2 level separation).[17]

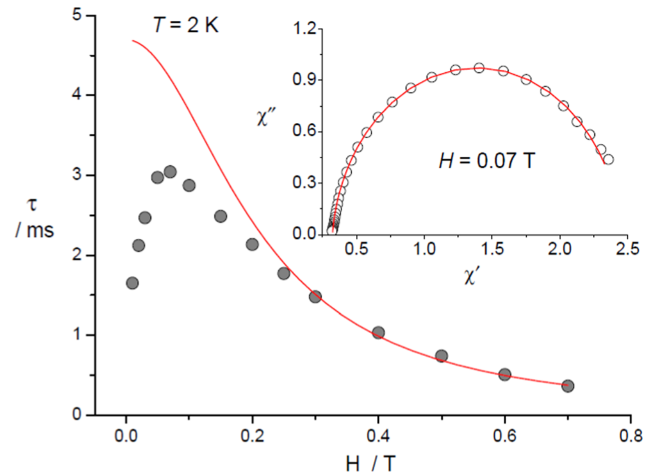

Figure 5. Field dependence of the relaxation time, τ, at 2 K determined from ac measurements. The line represents $\tau^{-1} \approx 5003H^2 + 213$ approximation (see text). Inset: Cole−Cole plot at 2 K for frequencies between 10 Hz and 10 kHz and the fit using the generalized Debye model (line).

The pronounced maximum on $\tau(H)$ at 2 K (Figure 5) shows that in **1** we deal with an interplay of two or more relaxation processes. In 0.2−0.7 T the field dependence of the spin−lattice relaxation rate $\tau^{-1}(H)$ can be approximated by the relation $\tau^{-1} \approx 5003H^2 + 213$ (Figure 5). The two components of this relation appear probably from the first- and second-order Raman relaxation processes, respectively.[18] For lower fields (H < ∼0.07 T) an effect responsible for the increase of the spin-flip rate $1/\tau$ is clearly noticeable.

In principle, in the case of Co^{II} with $D > 0$ the direct spin-phonon transitions within the lowest doublet are forbidden at H = 0 (due to the time-reversal symmetry of a Kramers doublet[18]), and only slow magnetic relaxations via higher energy levels can be expected. The absence of such relaxations in **1** in zero static magnetic field can be attributed to the fast ground-state spin-reversal QTM (for Kramers ions mediated by the dipolar or hyperfine interactions and already reported for both $D < 0$ and $D > 0$ Co^{II} single-ion systems[4a−c,g,h]). The application of the magnetic field suppresses the QTM (by means of the Zeeman effect) and slows down the spin-reversal process.

The log−log scale of τ^{-1} vs T dependence at 0.07 T (Figure 6) gives two linear ranges: 2−2.8 K described by $\tau^{-1} \sim T^{2.8}$ relation and 3.4−5 K described by $\tau^{-1} \sim T^{7.3}$. The lower temperature range ($\tau^{-1} \sim T^{2.8}$) may be explained in terms of

dx.doi.org/10.1021/ic501870h | Inorg. Chem. 2014, 53, 12870−12876

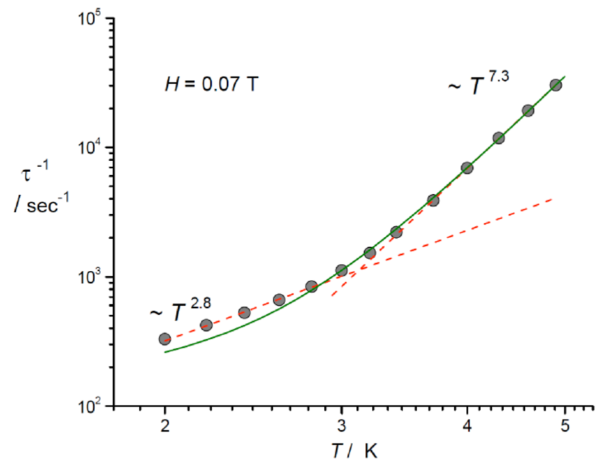

Figure 6. Thermal evolution of the relaxation rate, τ^{-1}, in a 0.07 T applied dc field (in log−log scale). The solid line represents $\tau^{-1} \approx 108.9T + 0.317T^7 + 0.005T^9$ approximation (see the text).

the dominating two-phonon optical acoustic Raman-like process,[19] which provides the $\tau^{-1} \sim T^n$ power law, where n = 1, 2, ..., 6 depending on the structure of the energy levels. A similar spin-phonon relaxation mechanism has been recently indicated by Colacio et al. in a Co^{II}−Y^{III} SIM.[4g] In turn, the higher temperature range with $\tau^{-1} \sim T^{7.3}$ dependence may reflect the two-phonon acoustic Raman processes ($\tau^{-1} \sim T^7$ and $\tau^{-1} \sim T^9$) or the exponential law $\tau^{-1} \sim \exp(-U_{eff}/k_BT)$ typical of the Orbach relaxation mechanism, as was indicated by the Arrhenius plot (inset in Figure 5). Observation of the one-phonon Orbach relaxations suggests the existence of the spin-reversal energy barrier. Usually such an energy barrier is expected in the systems with uniaxial magnetic anisotropy (D < 0). However, recently, Vallejo et al.[4c] proposed a model for which in a Co^{II} complex with D > 0 the significant transverse anisotropy, described by the $E[\hat{S}_x^{\,2} - \hat{S}_y^{\,2}]$ term, led to creation of a preferred axis within the xy easy plane. Taking into account the relatively large value of the rhombic ZFS parameter $|E|$ = 6.3 cm^{-1} obtained for **1**, we can assume a similar mechanism for formation of the in-plane anisotropy barrier that prevents the spin reversal (m_S = +1/2 to m_S = −1/2) and leads to the SIM-like behavior at $H \neq 0$. But, as was rightly noted by Gómez-Coca et al.,[4k] the Orbach relaxation mechanism does not fit well if the energy difference between the ground and excited Kramers doublets (~60 cm^{-1} in **1**) is significantly higher than the estimated activation energy barrier (~21.5 cm^{-1} in **1**).

A new approach in the interpretation of the slow relaxation effects in Kramers ion mononuclear complexes with positive ZFS was proposed very recently by Gómez-Coca et al.[4k] These authors have demonstrated that in the case of Co^{II} ions the hyperfine interactions breaks the time-reversal symmetry and enables the direct spin-phonon transitions between states of the ground doublets. However, at zero static magnetic field such relaxations are masked by the electronuclear spin entanglement. It was also shown that at sufficiently small fields the $\tau^{-1}(H)$ dependence of the overall relaxation rate of the system can be complicated by such subtle effect as the nuclear spin−lattice coupling. The dependence τ^{-1} vs T for **1** was fitted with the expression representing the sum of the direct and Raman processes. The best fit relation is $\tau^{-1} \approx 108.9T + 0.317T^7 + 0.005T^9$ (solid line in Figure 6), where the first component is ascribed to the direct one-phonon relaxations and two next to the first- and second-order two-phonon Raman processes.[18] The obtained relation describes the experimental $\tau^{-1}(T)$ quite well (especially at T > 3 K). The small divergence at T < 3 K, where the direct mechanism contributes, may indicate more complex magnetic relaxation processes in **1** at very low temperatures. The rate of Kramers one-phonon direct relaxations is expected to depend strongly upon static magnetic field ($\tau^{-1} \sim H^4$). But, for the Kramers ions, when the additional splitting of the ground-state doublet by the hyperfine interactions are taken into account, the $\tau^{-1} \sim H^2$ relation is expected.[18] Strikingly, the field dependence of the relaxation rates at 2 K fulfills this relation but only for larger fields, H > ~0.2 T (see the text above and Figure 5). At low fields the τ^{-1} vs H behavior can be modified by the contribution of such effects as dipolar interactions and nuclear spin−lattice coupling.[4k] Since the $\tau^{-1}(T)$ data were obtained in H = 0.07 T (<0.2 T), it is possible that the observed discrepancy of the experimental and fitted $\tau^{-1}(T)$ dependences (Figure 6) is the result of the subtle influence of the additional effects mentioned above.

Thus, the analysis performed indicates that in **1** the thermal dependences of the field-induced magnetic relaxation rate at T < 3 K can be quite well explained in the frame of the model proposed by Gómez-Coca et al.[4k] However, we cannot also exclude that two-phonon optical acoustic Raman-like relaxation processes are responsible at low temperatures for the observed $\tau^{-1}(T)$ dependence.[4g] At higher temperatures, T > 3 K, the two-phonon Raman spin−lattice relaxation mechanism seems to prevail anyway.

■ CONCLUSIONS

In summary, we developed a rational supramolecular approach to the construction of a γ-CD-templated system in which the CD ligand serves not only to keep magnetic ions in a well-defined network but also to enable their spatial separation in order to obtain independent single-ion magnets. The reported heterometallic dodecanuclear sandwich-type complex **1** with the {Co, Li, Li}$_4$ ring contains a grid of four magnetically isolated Co^{II} ions in trigonal bipyramidal geometry. We have shown that the individual Co^{II} ions (endowed with positive ZFS parameter D) exhibit field-induced slow magnetic relaxation consistent with SIM behavior. Moreover, we present one of the first detailed studies of slow magnetic relaxations in the trigonal bipyramidal Co^{II} geometry.

■ EXPERIMENTAL SECTION

Synthetic Materials and Methods. γ-Cyclodextrin (γ-CD) was purchased from Cavamax W8 Pharma. Commercially available (Sigma-Aldrich) cobalt chloride hexahydrate and lithium hydroxide monohydrate were used as received without further purification. Elemental analyses were performed on a Perkin-Elmer type 240 elemental analyzer. The concentration of metal ions was determined by ICP-OES, using an ARL model 3410 sequential spectrometer (Fisons Instruments). Thermogravimetric analysis experiments were performed under argon with a heating rate of 5 °C min^{-1} using a TA Instruments Q600 apparatus. Single-crystal X-ray diffraction data were collected at 100(2) K on a SuperNova Agilent diffractometer using Mo Kα radiation (λ = 0.710 73 Å). EPR spectra were collected with an EMX Bruker ER083CS spectrometer operating at a fixed frequency in X-band (9.382 GHz) and equipped with a liquid helium cryostat. The powdered sample was wrapped in a polyethylene membrane and fixed to the quartz holder.

Synthetic Procedure. Hydrated cobalt(II) chloride, $CoCl_2 \cdot 6H_2O$ (237.93 mg, 1.0 mmol), and γ-CD (470 mg, 0.362 mmol) were dissolved in water (4 mL) and slowly dropped at room temperature into a water suspension of monohydrated lithium hydroxide ($LiOH\cdot H_2O$; 945 mg, 22.5 mmol) and γ-CD (470 mg, 0.362 mmol). After 5 min, a clear, deep blue solution was filtered and carefully introduced to the vapors of acetone. Pink needle-like crystals were formed within 2 weeks and collected by filtration. Results of the elemental analysis of the bulk material were diverging due to difficulties with purification of the crude material from inorganic salt residues. The amount of cobalt(II) ions in the bulk material used in magnetic studies was determined by ICP-OES. Based on the elemental analysis and the single-crystal X-ray diffraction data, the formula of the resulting heterometallic dodecanuclear complex should be stated as $[(\gamma\text{-CD})_2Co_4Li_8(H_2O)_{12}]\cdot nH_2O$. The amount of water in **1** was confronted with the results of DSC/TG analysis for the bulk material (Figure S7).

Single-Crystal X-ray Diffraction. Single crystals of **1** with appropriate dimensions were chosen under an optical microscope and mounted in a nylon loop in a drop of silicon oil to prevent the possibility of decay of the crystal during data collection. The unit cell parameters were determined from 10 frames, then refined on all data. The data were processed with CrysAlisPro.[20a] The structure was solved by direct methods using SHELXS97[20b] and refined by full matrix least-squares on F^2 using SHELXL97.[20c] All non-hydrogen atoms were refined with anisotropic displacement parameters. CCDC-1006436 contains the supplementary crystallographic data for this paper. These data can be obtained free of charge from the Cambridge Crystallographic Data Centre via www.ccdc.cam.ac.uk/data_request/cif. Crystal data for **1**: $C_{96}H_{128}Co_4Li_8O_{114}$; M = 3397.22, crystal dimensions 0.24 × 0.20 × 0.10 mm^3, tetragonal, space group $P4$ (no. 75), a = 25.4682(9) Å, b = 25.4682(9) Å, c = 15.3628(6) Å, β = 108.814(2)°, U = 9964.8(6) Å^3, Z = 2, $F(000)$ = 3496, D_c = 1.132 g cm^{-3}, T = 100(2) K, μ(Mo Kα) = 3.983 mm^{-1}, θ_{max} = 26.37°, 20 079 unique reflections. Refinement converged at R_1 = 0.1663, wR_2 = 0.2426 for all data and 1000 parameters (R_1 = 0.0973, wR_2 = 0.1944 for 8371 reflections with $I_o > 2\sigma(I_o)$). The goodness-of-fit on F^2 was equal to 0.912. A weighting scheme $w = [\sigma^2(F_o{}^2 + (0.0418P)^2 + 3.1964P]^{-1}$ where $P = (F_o{}^2 + 2F_c{}^2)/3$ was used in the final stage of refinement. The residual electron density = +0.83/−0.53 e Å^{-3}. In the crystal structure of **1**, apart from 12 water molecules coordinated to metals, there are 54 disordered water molecules per molecule of **1**, as indicated by the SQUEEZE calculation method. To improve the geometrical parameters, the SQUEEZE function of PLATON (van der Sluis and Spek, 1990; Spek, 2001) was used to eliminate the contribution of the electron density in the solvent region from the intensity data.

Magnetic Measurements. Magnetic measurements were performed with a Quantum Design PPMS magnetometer equipped with a 9 T magnet. Magnetization curves were measured at selected temperatures in the accessible field range. Direct current (dc) magnetization (M) was determined as a function of temperature (in the range 2−298 K) in both zero-field-cooled (ZFC) and field-cooled (FC) regimes at 0.1 T applied magnetic field. Alternating current (ac) susceptibility measurements were carried out in an oscillating ac field of 3−5 Oe with frequencies from 10 Hz to 10 kHz. Variable-frequency and variable-temperature ac susceptibility data were collected under different applied dc fields selected from the range 0.01−0.7 T.

The magnetic measurements were performed on well-compressed powdered sample sealed in a PCV capsule to preclude the loss of incorporated water molecules when the sample was exposed to vacuum in the PPMS. The background signal of the sample holders was checked independently and subtracted from the measured data. The magnetic measurements data were also corrected for molecular diamagnetism using standard procedures.[21]

Computational Details. The magnetic susceptibility was numerically calculated using the known van Vleck equation. The values of energy levels at a given direction of the magnetic field were found by the exact numerical diagonalization of the spin-Hamiltonian given by eq (a). Finally, the averaged susceptibility $\chi_m = 1/3(\chi_x + \chi_y + \chi_z)$ was calculated. To take into account the van Vleck paramagnetism and inaccuracies in corrections for the holder and molecular diamagnetism, a constant χ_{TIP} was added to the final expression for magnetic susceptibility: $\chi_{calcd} = \chi_m + \chi_{TIP}$. The least-squares method was used to fit calculated susceptibility to experimental results. The agreement factor R was defined as $R = \sum(\chi - \chi_{calcd})^2/\sum\chi^2$.

Cole−Cole plots were fitted using the formulas describing χ' and χ'' as a function of frequency:

$$\chi'(\omega) = \chi_s + \frac{\chi_{TS}(1 + (\omega\tau)^{1-\alpha}\sin(\pi\alpha/2))}{1 + 2(\omega\tau)^{1-\alpha}\sin(\pi\alpha/2) + (\omega\tau)^{2(1-\alpha)}}$$

and

$$\chi''(\omega) = \frac{\chi_{TS}(\omega\tau)^{1-\alpha}\cos(\pi\alpha/2)}{1 + 2(\omega\tau)^{1-\alpha}\sin(\pi\alpha/2) + (\omega\tau)^{2(1-\alpha)}}$$

where $\omega = 2\pi\nu$ and $\chi_{TS} = \chi_T - \chi_S$ (χ_T and χ_S are the isothermal and adiabatic susceptibilities, respectively), τ is the relaxation time, and α is a variable representing the distribution of relaxation times.

ASSOCIATED CONTENT

Supporting Information

Selected magnetic and EPR data are given in the Supporting Information. CCDC 1006436 (**1**) contains the supplementary crystallographic data for this paper. This material is available free of charge via the Internet at http://pubs.acs.org.

AUTHOR INFORMATION

Corresponding Authors

*E-mail: slaws@ifpan.edu.pl.

*E-mail: lewin@ch.pw.edu.pl.

Author Contributions

‡N. Nedelko and A. Kornowicz contributed equally.

Notes

The authors declare no competing financial interest.

ACKNOWLEDGMENTS

We acknowledge the Foundation for Polish Science Team Program (project TEAM/2011-7/8) and the European Regional Development Fund (POIG.01.01.02.-14-102/09) for financial support. The research was partially performed in the laboratories funded by POIG.02.02.00-00-025/09.

REFERENCES

(1) (a) Gatteschi, D.; Sessoli, R.; Villain, J. *Molecular Nanomagnets*; Oxford University Press, 2006. (b) *Structure and Bonding: Single-Molecule Magnets and Related Phenomena*; Winpenny, R., Ed.; Springer-Verlag: Berlin, 2006; Vol. *122*. (c) *Molecular Magnets: Physics and Aplications*; Bartolomé, J.; Luis, F.; Fernandez, J. F., Eds.; Springer-Verlag: Berlin, 2014. (d) Aromí, G.; Aguilà, D.; Gamez, P.; Luis, F.; Roubeau, O. *Chem. Soc. Rev.* **2012**, *41*, 537−546.

(2) Miyasaka, H.; Nakata, K.; Lecren, L.; Coulon, C.; Nakazawa, Y.; Fujisaki, T.; Sugiura, K.; Yamashita, M.; Clérac, R. *J. Am. Chem. Soc.* **2006**, *128*, 3770−3783.

(3) (a) Zhang, P.; Guo, Y.-N.; Tang, J. *Coord. Chem. Rev.* **2013**, *257*, 1728−1763. (b) Zhang, P.; Zhang, L.; Wang, C.; Xue, S.; Lin, S.-Y.; Tang, J. *J. Am. Chem. Soc.* **2014**, *136*, 4484−4487. (c) Guo, Y.-N.; Ungur, L.; Granroth, G. E.; Powell, A. K.; Wu, C.; Nagler, S. E.; Tang, J.; Chibotaru, L. F.; Cui, D. *Sci. Rep.* **2014**, *4:5471*, 1−7.

(4) (a) Jurca, T.; Farghal, A.; Lin, P.-H.; Korobkov, I.; Murugesu, M.; Richeson, D. S. *J. Am. Chem. Soc.* **2011**, *133*, 15814−15817. (b) Zadrozny, J. M.; Long, J. R. *J. Am. Chem. Soc.* **2011**, *133*, 20732−20734. (c) Vallejo, J.; Castro, I.; Ruiz-García, R.; Cano, J.; Julve, M.; Lloret, F.; De Munno, G.; Wernsdorfer, W.; Pardo, E. *J. Am. Chem. Soc.* **2012**, *134*, 15704−15707. (d) Habib, F.; Luca, O. R.; Vieru, V.; Shiddiq, M.; Korobkov, I.; Gorelsky, S. I.; Takase, M. K.; Chibotaru, L. F.; Hill, S.; Crabtree, R. H.; Murugesu, M. *Angew. Chem., Int. Ed.* **2013**, *52*, 11290−11293. (e) Gómez-Coca, S.; Cremades, E.;

Aliaga-Alcalde, N.; Ruiz, E. *J. Am. Chem. Soc.* **2013**, *135*, 7010−7018. (f) Zhu, Y.-Y.; Cui, C.; Zhang, Y.-Q.; Jia, J.-H.; Guo, X.; Gao, C.; Qian, K.; Jiang, S.-D.; Wang, B.-W.; Wang, Z.-M.; Gao, S. *Chem. Sci.* **2013**, *4*, 1802−1806. (g) Colacio, E.; Ruiz, J.; Ruiz, E.; Cremades, E.; Krzystek, J.; Carretta, S.; Cano, J.; Guidi, T.; Wernsdorfer, W.; Brechin, E. K. *Angew. Chem., Int. Ed.* **2013**, *52*, 9130−9134. (h) Huang, W.; Liu, T.; Wu, D.; Cheng, J.; Ouyang, Z. W.; Duan, C. *Dalton Trans.* **2013**, *42*, 15326−15331. (i) Boča, R.; Miklovič, J.; Titiš, J. *Inorg. Chem.* **2014**, *53*, 2367−2369. (j) Herchel, R.; Váhovská, L.; Potočňák, I.; Trávníček, Z. *Inorg. Chem.* **2014**, *53*, 5896−5898. (k) Gómez-Coca, S.; Urtizberea, A.; Cremades, E.; Alonso, P. J.; Camón, A.; Ruiz, E.; Luis, F. *Nat. Commun.* **2014**, *5:4300*, 1−8.

(5) (a) Vallejo, J.; Pascual-Álvarez, A.; Cano, J.; Castro, I.; Julve, M.; Lloret, F.; Krzystek, J.; De Munno, G.; Armentano, D.; Wernsdorfer, W.; Ruiz-García, R.; Pardo, E. *Angew. Chem., Int. Ed.* **2013**, *52*, 14075−14079. (b) Ishikawa, R.; Miyamoto, R.; Nojiri, H.; Breedlove, B. K.; Yamashita, M. *Inorg. Chem.* **2013**, *52*, 8300−8302. (c) Grigoropoulos, A.; Pissas, M.; Papatolis, P.; Psycharis, V.; Kyritsis, P.; Sanakis, Y. *Inorg. Chem.* **2013**, *52*, 12869−12871.

(6) Poulten, R. C.; Page, M. J.; Algarra, A. G.; Le Roy, J. J.; López, I.; Llobet, A.; Macgregor, S. A.; Mahon, M. F.; Murphy, D. M.; Murugesu, M.; Whittlesey, M. K. *J. Am. Chem. Soc.* **2013**, *135*, 13640−13643.

(7) (a) Freedman, D. E.; Harman, W. H.; Harris, T. D.; Long, G. J.; Chang, C. J.; Long, J. R. *J. Am. Chem. Soc.* **2010**, *132*, 1224−1225. (b) Harman, W. H.; Harris, T. D.; Freedman, D. E.; Fong, H.; Chang, A.; Rinehart, J. D.; Ozarowski, A.; Sougrati, M. T.; Grandjean, F.; Long, G. J.; Long, J. R. *J. Am. Chem. Soc.* **2010**, *132*, 18115−18126. (c) Lin, P.-H.; Smythe, N. C.; Gorelsky, S. J.; Maguire, S.; Henson, N. J.; Korobkov, I.; Scott, B. L.; Gordon, J. C.; Baker, R. T.; Murugesu, M. *J. Am. Chem. Soc.* **2011**, *133*, 15806−15809. (d) Weismann, D.; Sun, Y.; Lan, Y.; Wolmershäuser, G.; Powell, A. K.; Sitzmann, H. *Chem.—Eur. J.* **2011**, *17*, 4700−4704. (e) Zadrozny, J. M.; Atanasov, M.; Bryan, A. M.; Lin, C.-Y.; Rekken, B. D.; Power, P. P.; Neese, F.; Long, J. R. *Chem. Sci.* **2013**, *4*, 125−138.

(8) Mossin, S.; Tran, B. L.; Adhikari, D.; Pink, M.; Heinemann, F. W.; Sutter, J.-P.; Szilagyi, R. K.; Meyer, K.; Mindiola, D. J. *J. Am. Chem. Soc.* **2012**, *134*, 13651−13661.

(9) (a) Fuchs, R.; Habermann, N.; Klüfers, P. *Angew. Chem., Int. Ed.* **1993**, *32*, 852−854. (b) Klüfers, P.; Piotrowski, H.; Uhlendorf, J. *Chem.—Eur. J.* **1997**, *3*, 601−608. (c) Geisselmann, A.; Klüfers, P.; Kropfgans, C.; Mayer, P.; Piotrowski, H. *Angew. Chem., Int. Ed.* **2005**, *44*, 924−927. (d) Benner, K.; Ihringer, J.; Klüfers, P.; Marinov, D. *Angew. Chem., Int. Ed.* **2006**, *45*, 5818−5822. (e) Hoshino, N.; Nakano, M.; Nojiri, H.; Wernsdorfer, W.; Oshio, H. *J. Am. Chem. Soc.* **2009**, *131*, 15100−15101. (f) Wei, Y.; Sun, D.; Yuan, D.; Liu, Y.; Zhao, Y.; Li, X.; Wang, S.; Dou, J.; Wang, X.; Hao, A. *Chem. Sci.* **2012**, *3*, 2282−2287. (g) Wei, Y.; Han, S.; Walker, D.; Fuller, P. E.; Grzybowski, B. *Angew. Chem., Int. Ed.* **2012**, *51*, 7435−7435. (h) Bagabas, A. A.; Frasconi, M.; Iehl, J.; Hauser, B.; Farha, O. K.; Hupp, J. T.; Hartlieb, K. J.; Botros, Y. Y.; Stoddart, J. F. *Inorg. Chem.* **2013**, *52*, 2854−2861.

(10) Boča, R. *Coord. Chem. Rev.* **2004**, *248*, 757−815.

(11) Notice that in the course of fitting attempts the sign of the E parameter depends on the choice of $x-y$ coordinate axes (with the z-direction defined along the apical bonds). Replacing x and y will require the change of E sign but has no effect on the goodness-of-fit.

(12) Makinen, M. W.; Kuo, L. C.; Yim, M. B.; Wells, G. B.; Fukuyama, J. M.; Kim, J. E. *J. Am. Chem. Soc.* **1985**, *107*, 5245−5254.

(13) Cucinotta, G.; Perfetti, M.; Luzon, J.; Etienne, M.; Car, P.-E.; Caneschi, A.; Calvez, G.; Bernot, K.; Sessoli, R. *Angew. Chem., Int. Ed.* **2012**, *51*, 1606−1610.

(14) Petit, S.; Pilet, G.; Luneau, D.; Chibotaru, L.; Ungur, L. *Dalton Trans.* **2007**, *40*, 4582−4588.

(15) Cole, K. S.; Cole, R. H. *J. Chem. Phys.* **1941**, *9*, 341−351.

(16) Schenker, R.; Leuenberger, M. N.; Chaboussant, G.; Loss, D.; Güdel, H. U. *Phys. Rev. B* **2005**, *72*, 184403.

(17) Zadrozny, J. M.; Liu, J.; Piro, N. A.; Chang, C. J.; Hill, S.; Long, J. R. *Chem. Commun.* **2012**, *48*, 3897−4020.

(18) Abragam, A.; Bleaney, B. *Electron Paramagnetic Resonance of Transition Ions*; Clarendon Press Oxford: Oxford, U.K., 1970.

(19) (a) Singh, A.; Shrivastava, K. N. *Phys. Status Solidi B* **1979**, *95*, 273−277. (b) Shrivastava, K. N. *Phys. Status Solidi B* **1983**, *117*, 437−458.

(20) (a) *CrysAlisPro*, Version 1.171.35.21b; Agilent Technologies, 2011. (b) Sheldrick, G. M. *Acta Crystallogr., Sect. A* **1990**, *46*, 467−473. (c) Sheldrick, G. M. *Acta Crystallogr.* **2008**, *64A*, 112−122.

(21) Bain, G. A.; Berry, J. F. *J. Chem. Educ.* **2008**, *85*, 532−536.